Variational theory of bulk ^{4}He with shadow wave functions: Ground state and the phonon-maxon-roton spectrum

S. Moroni
The Abdus Salam International Centre for Theoretical Physics, Strada Costiera 11, I-34014 Trieste, Italy

D. E. Galli
Istituto Nazionale di Fisica della Materia, via Celoria 16, I-20133 Milano, Italy
and Dipartimento di Fisica, Università degli Studi di Milano, via Celoria 16, I-20133 Milano, Italy

S. Fantoni
International School for Advanced Studies, Via Beirut 2/4, I-34014 Trieste, Italy

L. Reatto
Istituto Nazionale di Fisica della Materia, via Celoria 16, I-20133 Milano, Italy
and Dipartimento di Fisica, Università degli Studi di Milano, via Celoria 16, I-20133 Milano, Italy
(Received 6 February 1998)

We apply an efficient optimization scheme to shadow wave functions (SWF's) for the ground state of liquid and solid ^{4}He. Results improve on previous variational energies in both phases. In the liquid, the gain over a wave function with only pair and triplet correlations increases with density, providing a quantitative estimate of the increasing effect of higher-order correlations. The discrepancy with the exact ground-state energy is nearly constant over a wide range of densities, yielding excellent estimates for the equilibrium, freezing, and melting densities. The optimal SWF's can be represented with high precision by density-independent sets of variational parameters for the liquid and the solid phases. An extensive study of ground-state properties demonstrates the uniformly good quality of the variational description afforded by the optimized SWF's. Based on such an accurate representation of the ground state, and including the correct long-range correlations due to the zero-point motion of phonons, we compute the excitation spectrum and the strength of the single quasiparticle excitation peak. While the use of optimized SWF's confirms the accuracy of previous studies in the maxon-roton region, the proper treatment of long-range correlations allows us to extend to the phonon region the agreement between theory and experiment. We simulate relatively large systems in order to explore the long-wavelength regime in detail. Even down to wave vectors where the excitation energy exhibits a highly linear dispersion, which would suggest a harmonic phonon mode, the kinetic and potential energies of the excitation are far from verifying equipartition. This result is supported by additional diffusion Monte Carlo simulations within the fixed node approximation. We locate the onset of the harmonic regime for the long-wavelength excitations at an extremely small value of the wave vector, $k \lesssim 0.05$ Å^{-1}.
[S0163-1829(98)00126-X]

I. INTRODUCTION

The variational theory of strongly interacting bosons, like the condensed phases of ^{4}He, has been developed to a high level and it has reached a good accuracy at least for the ground state[1,2] at the equilibrium density. Fully optimized forms for the ground-state wave functions Ψ have been obtained when the interparticle correlations in Ψ have been truncated to the three-body level, i.e., Ψ contains two-body (Jastrow) and triplet terms. Computations based on Euler-Lagrange equations within hypernetted chain schemes[1] as well as on Monte Carlo basis set optimization[2] have been performed. The saturation density of liquid ^{4}He is in fairly good agreement with experiment and with results of exact stochastic methods and the variational binding energy is about 0.2 K above the correct value,[2] with a deviation of 3%. The accuracy decreases at higher density and in fact the deviation reaches about 8% at the freezing density. This has been taken as an indication that correlations beyond the three-body level become important at such high density. As one moves into the solid and Ψ is augmented by localizing factors, one regains accuracy in the energy with a deviation from the correct value of order of 0.2 K.

Much less satisfactory is the situation with the excited states. With the method of correlated basis functions the excited states wave function $\Psi_{\mathbf{k}}$ of momentum $\hbar\mathbf{k}$ is written as a product $\Psi_{\mathbf{k}}=F_{\mathbf{k}}\Psi$ of the ground state Ψ_0 and of an excitation operator $F_{\mathbf{k}}$. $F_{\mathbf{k}}$ is expressed as a polynomial in the density-fluctuation operators $\{\rho_{\mathbf{k}}\}$. At lowest order $F_{\mathbf{k}}$ simply coincides with $\rho_{\mathbf{k}}=\Sigma_j \exp(i\mathbf{k}\cdot\mathbf{r}_j)$ and this represents the Feynman form for the excited states.[3] Terms beyond the linear one introduce the so-called backflow effects. In a different, but related, approach, the least action principle is used in a time-dependent form of wave function.[4] This last theory has been developed up to the level corresponding to one-body and two-body time-dependent correlations. Within such methods a number of approximations have to be introduced and this affects the reliability of the results. Sometimes even

an adjustable parameter has been introduced such that the roton energy, for instance, is in agreement with experiments.[5] Results obtained under controlled approximation give a roton energy that is in the range of 10 K at equilibrium density, almost 20% above experiment and the results are even poorer at higher density. Also, the few computations of the strength $Z(k)$ of the single excitation peak in the dynamical structure factor $S(k,\omega)$ show a large discrepancy from the experimental neutron-scattering results.[6,7]

An alternative approach has been developed in the variational theory of strongly interacting bosons; the method of shadow wave function (SWF) (Refs. 8, 9 and 10). Here correlations beyond the pair level are introduced by coupling the position variables of the particles to subsidiary variables, the shadow variables. This wave function contains three pair correlating factors (in terms of their logarithms, three pseudopotentials), the particle-particle, the particle-shadow, and the shadow-shadow one. Integration over the subsidiary variables introduces in an implicit way effective correlations between the particles and these correlations are not limited to pair or triplet terms but terms at all orders are generated. Different motivations for such representation of the ground-state wave function have been presented. In one of these, each shadow variable associated to a particle is interpreted as a way to represent in the ground state the excluded volume due to the zero-point motion of the hard core particle.[11] The initial motivation for introducing the SWF has been that it describes the crystalline phase without explicitly breaking the translational invariance of the wave function: localization of particles is obtained via interparticle correlations.[8] It turns out that inclusion of physically motivated attractive correlations in the shadow-shadow pseudopotential leads to a rather accurate ground-state energy also in the liquid phase.[10] However, whereas optimization of the particle-particle pseudopotential has been already achieved, a full optimization of the SWF was never attempted. This made somewhat incomplete the comparison between SWF and the optimized Jastrow plus triplet wave function and unassessed the full extent of the role of correlations beyond the triplet level.

The interest in the SWF method[11] has been strongly enhanced by the discovery that this formalism could be extended in a natural way to treat excited states like the phonon-roton excitation branch[12] or a vortex line.[13] For instance, by the simple provision that the momentum carrying factor in $\Psi_{\mathbf{k}}$ is a density fluctuation in the subsidiary variables, one has a parameter-free wave function that gives a roton energy at the level of the best correlated basis function results. The explanation of such a good result is that switching the density fluctuation from the particle to the subsidiary variables allows for the presence of backflow effects in the particle variable. In addition, this backflow is represented by terms to all orders in the density fluctuation $\{\rho_{\mathbf{k}}\}$ of the real variables.[14] In a similar way, writing the phase factors for a vortex line in terms of the subsidiary variables allows for the backflow effects and for a delocalized vorticity and also in this case a strongly improved description of the vortex line is obtained in terms of a lower excitation energy.[15]

In the present paper we address in the first place the problem of a full optimization of the SWF, both in the liquid and in the solid phase. The first motivation is to assess in the liquid phase the role of correlations beyond the triplet level and, in the solid phase, to perform a detailed comparison between a wave function without explicitly broken translational symmetry like the SWF and the standard wave function with localizing factors. In the second place, an accurate ground-state wave function is a preliminary step in the study of excited states. Careful optimization of the ground state is important in order to be sure that information on the excited states are not biased by an inadequate ground state. Furthermore, we include the long-range part of the correlations due to the zero-point motion of phonons.

Starting from this optimized SWF we also study the phonon-maxon-roton excited states in the liquid phase. The goal is to verify to what extent the excellent results that were obtained with a less accurate representation of the SWF ground state[16,17] remain valid when the optimized SWF ground state is used. Previous results in the maxon and in the roton regions were in excellent agreement with experiment. The situation was less satisfactory in the high-frequency phonon region.[16,17] Another motivation for the present computation is to verify if the inclusion of the long-range correlations in the ground state is important to obtain the correct description of the phonon excitations. Finally, the computations of Refs. 16 and 17 gave a rather unexpected result: for high-frequency phonons equipartition between kinetic and potential energy as expected for long-wavelength phonons was not observed. In order to verify if this is an artifact of the SWF, we supplement the variational computation with a diffusion Monte Carlo (DMC) simulation with fixed nodes.

The contents of the paper are as follows. In Sec. II the optimization procedure of the SWF is described and the results for the energy, correlations, and Bose-Einstein condensate are presented. In Sec. III the method of computation for the excited states in the liquid phase is presented and the results for the excitation spectrum and for the strength of the single excitation peak in $S(k,\omega)$ are given. In this section the results for high-energy phonons as given by SWF and by DMC are also presented. Section IV is left for the conclusions.

II. WAVE-FUNCTION OPTIMIZATION AND GROUND-STATE PROPERTIES

The SWF is a trial function introduced for variational Monte Carlo studies of ground-state properties of liquid and solid ^{4}He. Formalism and applications are reviewed in Ref. 11. For the ground state of a homogeneous system of N bosons, we write the SWF in the form

$$\Psi(R)=\Phi_p(R)\int \Theta(R,S)\Phi_s(S)dS. \tag{1}$$

Here $R=\{\mathbf{r}_1,\ldots,\mathbf{r}_N\}$ are the coordinates of the particles, $S=\{\mathbf{s}_1,\ldots,\mathbf{s}_N\}$ is a set of auxiliary (shadow) variables, Φ_p and Φ_s are Jastrow pair products of particle and shadow coordinates, respectively, and $\Theta(R,S)=\exp[-\Sigma_i u_{sp}(|\mathbf{r}_i-\mathbf{s}_i|)]$ is a coupling function between particles and shadows. Early SWF calculations used a McMillan form[8] for both the pseudopotential u_p entering the Jastrow factor $\Phi_p=\exp[-\Sigma_{i<j}u_p(r_{ij})]$ and for the (similarly defined) shadow pseudopotential u_s. A Gaussian has been used so far for the shadow-particle coupling.

TABLE I. Energy per particle in K of liquid and fcc solid ^{4}He. For the variational results, OJOT(G) denotes a Feenberg function with optimal pair and triplet correlations, times a Gaussian one-body factor in the solid; $O2B+A(S)$ is a SWF with optimized particle correlations; $OSWF_0$ is the optimized SWF obtained from the basis set expansion, and OSWF the density-independent fitted form given in Eq. (8). The last column lists the nominally exact DMC results. All calculations use the *HFDHE2* potential (Ref. 18).

ρ (Å^{-3})	OJOT(G)	$O2B+A(S)$	$OSWF_0$	OSWF	DMC
			Liquid		
0.0196	−6.854(2) [a]	−6.695(27) [b]	−6.81(2)	−6.765(8)	−7.012(2) [a]
0.0207				−6.886(6)	−7.111(5) [a]
0.0218	−6.901(4) [a]	−6.789(23) [b]	−6.95(2)	−6.937(6)	−7.143(4) [a]
0.0229				−6.913(6)	
0.0240				−6.811(5)	−7.017(6) [a]
0.0251				−6.634(7)	
0.0262	−5.991(8) [a]	−6.286(22) [b]	−6.38(2)	−6.350(6)	−6.557(10) [a]
			fcc solid		
0.0293	−5.51(1)	−5.414(11) [b]	−5.55(2)	−5.566(5)	−5.759(6)
0.0303				−5.237(6)	
0.0313				−4.815(4)	−5.009(5)
0.0323				−4.319(6)	
0.0329		−3.765(12) [b]	−4.06(2)		
0.0335	−3.70(1)		−3.71(3)		
0.0343				−3.092(7)	
0.0353	−2.40(1)	−2.132(12) [b]	−2.40(2)	−2.339(8)	−2.641(6)

[a]Reference 2.
[b]Reference 10.

We remind that a SWF has the ability to describe both liquid and crystalline phases within the same functional form featuring Bose symmetry and translational invariance, whereas the Feenberg wave functions that have to be supplemented with a Nosanow one-body factor in the solid phase. In addition, integration over shadow coordinates implicitly introduces correlations between particles at all orders.

A natural question arises as to whether the SWF, beyond its appealing formal properties, also provides a quantitatively accurate variational description of the condensed phases of ^{4}He. Recently, a major improvement in the energy upper bounds has been achieved using the so-called $O2B+A(S)$ SWF,[10] which features (i) the physically motivated inclusion of an attractive part in the shadow pseudopotential u_s and (ii) the full numerical optimization of the particle-particle pseudopotential u_p. However, this $O2B+A(S)$ wave function gives relatively too little binding in the low-density liquid and in the high-density solid, which results in a poor equation of state. Furthermore, as shown in Table I, it is not as accurate as a Feenberg form with optimized two- and three-body correlations times a Nosanow Gaussian factor in the solid phase, which we will call OJOT(G), except in the liquid close to freezing where the quality of the OJOT wave function is severely limited by the neglect of higher-order correlations.[2]

In this section we discuss the extension of the numerical optimization procedure to *all* the pseudopotentials u_p, u_s, and u_{sp}. Despite the fact that a full optimization proves impossible using standard techniques, we manage to get the *best energy upper bounds* for both the liquid and the solid. Even more important, the discrepancy between the variational and the exact ground-state energy is nearly constant in the whole density range considered, yielding an *extremely good equation of state*, including excellent estimates for the equilibrium, freezing, and melting densities. The treatment of long-range correlations is also discussed.

A. Optimization procedure

The SWF optimization is carried out for systems of $N=64$ atoms in the liquid phase or $N=108$ atoms in the fcc solid with periodic boundary conditions. The use of these relatively small systems is justified by additional calculations for $N=180$ and 256 for the liquid at equilibrium density, which gave neither a significant improvement of the energy nor a sizeable change of the correlation functions. As usual, the shadow and the particle pseudopotentials are smoothly cutoff at a distance corresponding to half the simulation box side.[19] The Hamiltonian is

$$H=-\frac{\hbar^2}{2m}\nabla^2+V(R)=-\frac{\hbar^2}{2m}\sum_{i=1}^{N}\nabla_i^2+\sum_{i<j=1}^{N}v(r_{ij}), \quad (2)$$

where $v(r)$ is the *HFDHE2* Aziz potential.[18]

We adopt a computationally efficient scheme previously used to fully optimize two- and three-body correlations in a Feenberg wave function for liquid ^{4}He and ^{3}He.[2] *All* the pseudopotentials of the SWF are expanded according to $u_x(r)=u_x^0(r)[1+\Sigma_\mu a_x^\mu b_x^\mu(r)]$, where x is either p, s, or sp, and the basis functions $b_x^\mu(r)$ are Fourier components defined in the appropriate range of interparticle distances with suitable boundary conditions. The reference functions u_x^0, which correspond to the $M+A(S)$ SWF of Ref. 10, are McMillan, scaled Aziz, and harmonic pseudopotentials for the

particle, shadow, and particle-shadow correlations, respectively. Twenty basis functions b_x^μ for each pseudopotential are more than adequate. A linear combination Σ^2 of the total energy and its variance is minimized with respect to the coefficients a_x^μ using the reweighting method and taking advantage of the linearity in the variational parameters of $\ln\Psi$.[2]

Since the procedure is described in detail elsewhere,[2] we only need to establish the notation to discuss a couple of specific points for the implementation with the SWF. Briefly, a step of the reweighting method[20] consists of (i) sampling a set of M configurations from the square of a wave function with variational parameters $\mathbf{a}_0$, and (ii) using this fixed set to estimate the quantity Σ^2 for *different* choices of the variational parameters $\mathbf{a}$. We recall that when sampling the square of the SWF $\Psi(R)$, also the integrals over the shadow variables are done stochastically;[8] this introduces N ''left'' shadow S^L and N ''right'' shadow S^R, so that a configuration is defined by $X=\{R,S_L,S_R\}$. The quantity we minimize is thus

$$\Sigma^2(\mathbf{a})=\frac{\sum_i^M [E_{\not}(\mathbf{a};X_i)-\bar{E}]^2 W(X_i)}{\sum_i^M W(X_i)}, \tag{3}$$

where the *local energy* is given by[8]

$$\begin{aligned} E_{\not}(\mathbf{a};X) &= \frac{H\Psi(X)}{\Psi(X)} \\ &= V(R)-\frac{\hbar^2}{2m} \\ &\quad\times \frac{\nabla^2\Phi_p(R)[\Theta(R,S_L)+\Theta(R,S_R)]}{\Phi_p(R)[\Theta(R,S_L)+\Theta(R,S_R)]}, \end{aligned} \tag{4}$$

and the *weights* are given by

$$W(\mathbf{a};X)=\frac{\Phi_p^2(R)\Theta(R,S_L)\Theta(R,S_R)\Phi_s(S_L)\Phi_s(S_R)}{\Phi_{p;0}^2(R)\Theta_0(R,S_L)\Theta_0(R,S_R)\Phi_{s;0}(S_L)\Phi_{s;0}(S_R)}. \tag{5}$$

The subscript 0 in the last equation denotes the wave function with parameters $\mathbf{a}_0$, from which the X_i are sampled. The constant $\bar{E}$ in Eq. (3) tunes the weight with which the average of the local energy and its variance enter their linear combination Σ^2. The wave function Ψ with the parameters $\mathbf{a}$ that minimizes $\Sigma^2(\mathbf{a})$ is then used to generate a new set of configurations and the procedure is iterated to convergence.

Use of reweighting allows one to explore accurately and efficiently the parameter space, provided $\mathbf{a}$ is not too far from the values $\mathbf{a}_0$ used for the sampling. This ''distance'' in parameter space is measured in terms of the dispersion of the weights $W(X_i)$: a large dispersion implies that only few configurations contribute to the sums in Eq. (3), giving an estimate for Σ^2 with poor statistics. If the dispersion exceeds a prefixed threshold, the minimization routine is stopped and a new iteration of the reweighting procedure is started.

For each iteration we use $M\sim 10\,000$ statistically-independent configurations generated with a generalized Metropolis algorithm. In order to reduce the strong autocorrelations along the random walk, typical of the scaled Aziz SWF,[10] we first move the ith particle once sampling a Gaussian centered at $(\mathbf{s}_i^L+\mathbf{s}_i^R)/2$, and then the ith ''left'' and ''right'' shadows three times sampling Gaussians centered at $\mathbf{r}_i$, all the Gaussians having widths tuned to achieve the optimal acceptance rates.

The finite number of configurations used for the reweighting gives a statistical bias to the optimal variational parameters. If we keep iterating the optimization procedure after convergence, the energy fluctuates within 1 to 3×10^{-2} K, depending on the phase and the density of the system. This is our estimate for the accuracy on the energy of the ''optimal'' wave function.

One often uses variance minimization rather than energy minimization,[21] exploiting the zero variance principle of the local energy (namely, if Ψ is an exact eigenstate of H then $H\Psi(R)/\Psi(R)$ is obviously a constant). The SWF, on the other hand, does not have a zero variance principle, because the local energy of Eq. (4) contains fluctuations from the (unavoidable) sampling of the shadow variables. We nevertheless *must* give some weight to the variance in Σ^2 because we saw that an unconstrained minimization of the energy would lead to an uncontrolled increase of the variance, particularly in the liquid at low density.

A more serious drawback is the inadequacy of standard reweighting for the optimization of a highly parametrized form for the shadow pseudopotential u_s. The reason is that the growth of the dispersion of the weights $W(X_i)$ upon variation of the parameters $\mathbf{a}$ is much faster than the corresponding change of Σ^2: with the number of configurations M we use, the change in Σ^2 that we can induce in a step of the reweighting procedure by varying u_s is not statistically meaningful.

In some cases a similar problem has been circumvented[22] by setting all the weights $W(X_i)$ in Eq. (3) equal to 1. To test this possibility we have to use an estimator for the local energy which, unlike the one shown in Eq. (4), explicitly contains Φ_s (since the dependence of Σ^2 on Φ_s through the weights has to be suppressed). Such an estimator can be obtained by simply taking R and R-S as independent variables in Eq. (1). Unfortunately, the variance of this new estimator is so large that its use in the optimization scheme has not been useful.

In conclusion, we can fully optimize, under the constraint that the variance remains within an acceptable level, the particle pseudopotential u_p and the particle-shadow coupling u_{sp}. A much larger computational effort, or a better algorithm, would be needed to effectively optimize the shadow pseudopotential and the present results only represent a partially optimized shadow pseudopotential. In any case, our results give a rigorous upper bound to the energy and no bias is introduced.

B. Results

The optimized correlation factors $f_x(r)=\exp[-u_x(r)]$ (solid line) are displayed in Fig. 1, together with their values f_x^0 in the $M+A(S)$ function (dashed), for the case of liquid ^{4}He at equilibrium density. The optimal particle correlation f_p behaves like in the OJOT Feenberg wave

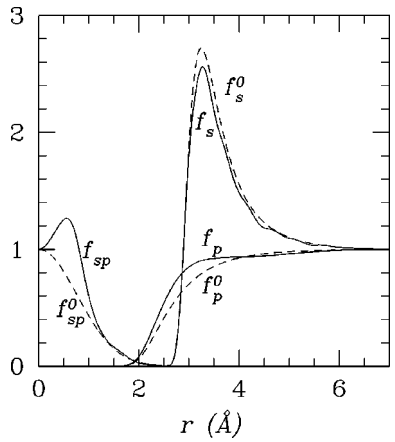

FIG. 1. Optimized correlation functions f_x (solid line) and their values f_x^0 before optimization (dashed) as a function of interparticle distance, for liquid ^{4}He at equilibrium density.

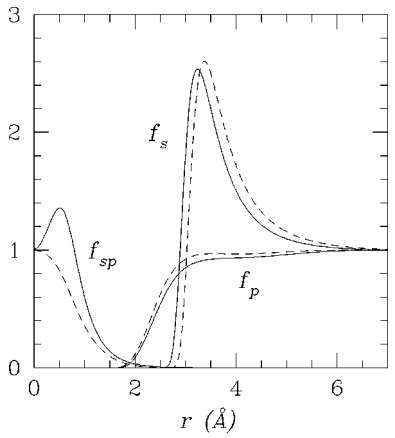

FIG. 2. Density-independent fits for the optimized correlation functions f_x of the liquid (full line) and the solid (dashed) as a function of interparticle distance.

function[2] or in the $O2B+A(S)$ SWF.[10] The irregular wavy behavior of the shadow correlation f_s is due to the problem discussed at the end of the previous section, and the difference from f_s^0 is probably not particularly meaningful.

The really new result is the optimized particle-shadow correlation, which sharply peaks at nonzero distance. Modification of the simple Gaussian f_{sp}^0 could be expected on the grounds of the path-integral analogy with improving the free-particle approximation to the density matrix, but the size of the effect was totally unanticipated. In the solid phase, the shape of f_{sp} is still non-Gaussian, but the peak is strongly suppressed (see Fig. 2).

In order to offer a more transferable representation of the optimized pseudopotential than given by the basis set expansion, we fit them to simpler expressions:

$$f_p(r)=\exp\left[-\left(p_1\exp[-p_2(r-p_3)^2]+p_4\exp[-p_5(r-p_6)^2]+\frac{p_7}{\epsilon+r^{p_8}}\right)\right], \tag{6}$$

$$f_{sp}(r)=\frac{\exp[-(p_1 r)^2]}{p_2+p_3r^2+p_4r^3+p_5r^4+p_6r^5+p_7r^6}, \tag{7}$$

$$f_s(r)=\exp\left[-\left(-\frac{p_1^6}{\epsilon+r^6}-\frac{p_2^8}{\epsilon+r^8}+\frac{p_3^{10}}{\epsilon+r^{10}}+\frac{p_4^{12}}{\epsilon+r^{12}}+\frac{p_5^{14}}{\epsilon+r^{14}}+\frac{p_6^{16}}{\epsilon+r^{16}}\right)\right]. \tag{8}$$

The constant $\epsilon=0.1$ is used to regularize the correlation functions at the origin.

It turns out that the density dependence of the optimized f_x's is very weak within either the solid or the liquid phase. For this reason we only fit one set of parameters for each phase. The fitted parameters are listed in Table II, and the resulting correlation functions f_x are shown in Fig. 2. We will denote by OSWF_0 the original optimized SWF given in terms of the basis set expansions, and by OSWF the fitted form of Eqs. (8).

The energies found with the OSWF_0 are listed in Table I, together with previous variational and DMC results, at various densities in the liquid and solid phases. Comparison is made with the nominally exact results of DMC simulations, rather than with the experimental equation of state, because we want to assess the accuracy of the variational calculation rather than the reliability of the model potential. The improvement over the best previous SWF calculation ($O2B+A(S)$, Ref. 10) is significant, ranging from about 0.1 K in the liquid to almost 0.3 K at the highest density considered in

TABLE II. Variational parameters. Lengths are in Å.

	Liquid			Solid		
	f_r	f_{rs}	f_s	f_r	f_{rs}	f_s
p_1	0.865 51	−0.466 76	2.554 76	10.654 90	−0.625 20	3.733 34
p_2	1.772 76	0.994 03	3.874 94	0.902 98	1.003 19	2.609 14
p_3	1.618 82	−3.824 17	3.669 45	0.627 07	0.289 43	3.013 89
p_4	0.055 71	6.858 91	2.213 21	0.034 31	−1.127 69	3.077 20
p_5	0.607 52	−3.677 84		0.868 45	3.722 18	3.016 15
p_6	4.194 70	0.985 46		4.081 23	−2.706 78	2.952 80
p_7	204.646 74			639.605 88	0.705 99	
p_8	6.838 99			11.427 01		

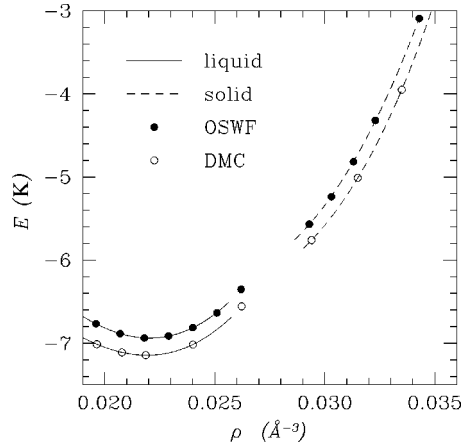

FIG. 3. Equation of state of ^{4}He at $T=0$. Lines are broken across the coexistence region.

the solid. The $OSWF_0$ also outdoes the OJOT Feenberg wave function.[2] The difference is small at the equilibrium density, but grows rapidly in the liquid as the density increases, showing that correlations beyond triplets, whose importance increases with density in the liquid, are effectively accounted for in the $OSWF_0$. In quantitative terms, these effects can be roughly estimated as follows. Comparison between the results of optimized Jastrow and OJOT shows that triplet correlations lower the energy by 0.8 K at ρ_{eq} and by 1 K at freezing density. The $OSWF_0$ gains 0.05 K over OJOT at ρ_{eq} and this is a lower bound for the contribution of correlations beyond the triplet level. In fact, we may suspect that in $OSWF_0$ the triplet correlations are not fully optimized because it is likely that by the present SWF one cannot generate an arbitrary form of triplet correlations. Said in different terms, we expect that a further (small) improvement in the energy will be obtained if the $OSWF_0$ is supplemented by an explicit triplet term. In support of this argument we note that the $OSWF_0$ energy is slightly above the OJOT result at the lowest density of the present computation, about 10% below ρ_{eq}. This suggests that the actual contribution of correlations beyond the triplet level in $OSWF_0$ is of order of 0.1 K at ρ_{eq}, i.e., about $\frac{1}{8}$ of the triplet contribution. At freezing density, correlations beyond the triplet level give at least a contribution equal to 0.4 K, $\frac{1}{3}$ of the triplet contribution, and this shows how rapidly these high-order correlations increase with density. In the solid phase at high density, $OSWF_0$ and OJOTG give essentially equivalent results. At melting density, the SWF gives an energy that is 0.07 K below the OJOTG result. This last wave function is not properly Bose symmetric and the only computation[23] in which the localizing Gaussians have been symmetrized as a permanent (i.e., a symmetrized product) of Gaussians gave an increased energy. This shows that a SWF gives a significantly improved description also of a low-density solid. It is not known if this improvement is due to non-Gaussian effects or to correlations beyond the triplet level. The geometry of the simulation cell and the periodic boundary conditions dictate the kind of ordered crystalline phase can be obtained with a SWF and in the present computation we have only studied the fcc crystal. It is useful to notice that recently it has been found[24] that within the SWF the stable solid phase is the hcp crystal, in agreement with experiment.

TABLE III. Fit parameters of the equation of state.

	Liquid		Solid	
	OSWF	DMC	OSWF	DMC
E_0	−6.9378	−7.1443	−6.2100	−6.5116
B	14.9101	13.2590	19.4387	0.0028
C	8.2699	9.7102	6.6727	13.5286
ρ_0	0.0220	0.0219	0.0249	0.0213

TABLE IV. Equilibrium, freezing, and melting densities in Å^{-3}.

	OSWF	DMC	Expt.
ρ_{eq}	0.0220	0.0219	0.0218
ρ_{fre}	0.0256	0.0258	0.0258
ρ_{mel}	0.0286	0.0290	0.0280

Table I also lists the energies calculated with the fitted OSWF. It appears that using a density-independent form in each phase (that may be very convenient for the simulation of inhomogeneous systems) does not downgrade severely the quality of the wave function.

The difference between the OSWF energies and the DMC results is almost constant in the whole density range considered, which means that the equation of state is well reproduced. The OSWF and DMC equations of state are shown in Fig. 3. The lines are cubic fits of the form

$$E(\rho)=E_0+B[(\rho-\rho_0)/\rho_0]^2+C[(\rho-\rho_0)/\rho_0]^3 \qquad (9)$$

to the calculated energies. The parameters of the fit are reported in Table III. From the fitted equation of state we calculate the equilibrium, freezing, and melting densities, and list them in Table IV. The agreement between OSWF and DMC is excellent. Also the pressure and the chemical potential computed from the OSWF equation of state, shown in Fig. 4, compare favorably with the exact results. Only in doubly differentiated quantities, such as the sound velocity and the compressibility (Fig. 5) do some discrepancies become evident.

We conclude this section with a comparison of OSWF and DMC results for quantities that are not directly derived from the total energy. In this case the DMC results are *extrapolated estimators*[20] and are biased by the trial function

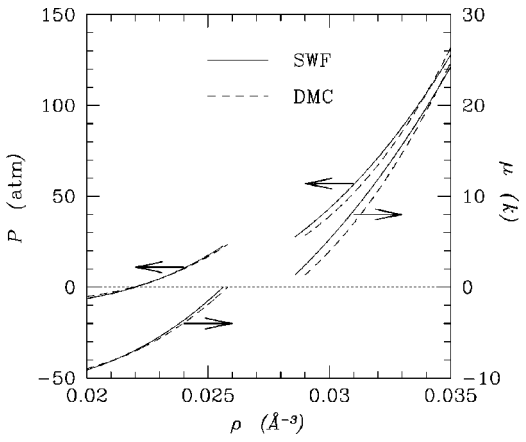

FIG. 4. Pressure P and chemical potential μ.

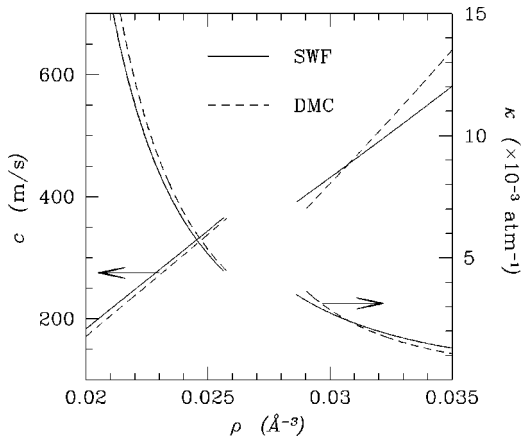

FIG. 5. Sound velocity c and compressibility κ.

adopted in the simulation. The comparison is therefore a less stringent test, but the uniformly good agreement found is nevertheless a meaningful assessment of the global good quality of the OSWF.

We show in Fig. 6 the pair distribution function $g(r)$ and list in Table V the kinetic energy. The one-body density matrix $n(r)$ is calculated as described in Ref. 8, except that the normalization is not determined by matching different estimators for large and short distances, but simply fitting the known normalization and curvature at the origin,

$$n(r)=1-\frac{mT}{3\hbar^2}r^2+O(r^3),$$

where T is the kinetic energy. The uncertainty in the normalization is less than 1% in the present calculation. The condensate fraction, computed as the average of $n(r)$ for $r>4.5$ Å, is listed in Table VI together with the results of other simulations. A statistical error is reported in the table. However, there is probably larger uncertainty due to the way of calculating n_0 from the one-body density matrix $n(r)$: for example, the results of OJOT and DMC are fitted to simulation data for both $n(r)$ and its Fourier transform $\hat{n}(k)$, the momentum distribution, *assuming* a particular functional

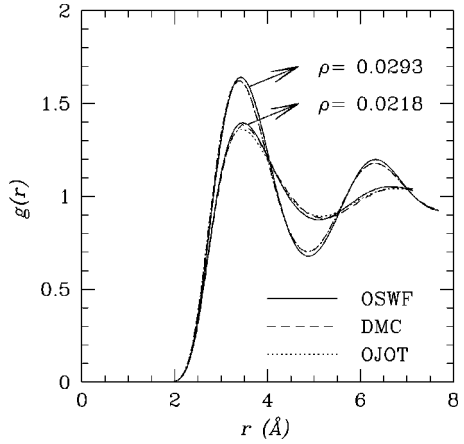

FIG. 6. Comparison between the OSWF, OJOT, and DMC results for the pair distribution function at the equilibrium density in the liquid, 0.0218 Å^{-3}, and at the melting density in the solid, 0.0293 Å^{-3}.

TABLE V. Kinetic energy per particle in K of the liquid and fcc solid. The OJOT and DMC data for the liquid are taken from Ref. 2.

ρ (Å^{-3})	OJOT	OSWF	DMC
		Liquid	
0.0196	11.936(7)	12.377(10)	11.688(11)
0.0207	13.069(7)	13.393(7)	12.881(21)
0.0218	14.233(8)	14.506(6)	14.049(18)
0.0229		15.702(6)	
0.0240	16.846(8)	16.997(6)	16.428(23)
0.0251		18.369(7)	
0.0262	19.639(13)	19.822(10)	19.312(26)
		fcc solid	
0.0293	25.53(2)	25.793(9)	25.040(47)
0.0303		27.428(7)	
0.0313		29.065(9)	28.128(33)
0.0323		30.683(11)	
0.0343		33.891(13)	
0.0353	35.15(2)	35.444(12)	34.454(43)

form;[25] the OSWF$_0$ result, and probably all the others, are obtained by averaging $n(r)$ on some ''large r'' range. Note that DMC and Green-function Monte Carlo are equivalent ''exact'' algorithms, the difference in the results being due to the bias on the extrapolated estimators from different trial wave functions (DMC uses OJOT). The path-integral Monte Carlo result has no systematic bias, but is calculated for a temperature of 1.18 K.

C. Long-range correlations

All the above results are obtained using short-range pseudopotentials. Actually, it is known[26] that the zero-point motion of long-wavelength phonons induces in the wave function a long-range r^{-2} correlation. This issue is particularly relevant in the present work that aims at a realistic characterization of the excitation spectrum, *including* phonons.

TABLE VI. Condensate fraction in ^{4}He from various calculations. Densities in Å^{-3}.

		$\rho=0.0218$	$\rho=0.0262$
VMC	M+M(S) [a]	0.0451(3)	
	M+A(S) [a]	0.077(5)	
	O2B+A(S) [a]	0.081(4)	
	OJOT	0.0869(4)	0.0415(3)
	OSWF$_0$	0.081(1)	0.036(1)
GFMC [b]		0.092(1)	0.037(2)
DMC [c]		0.0717(5)	0.0271(6)
PIMC [d]		0.069(10)	

[a]Reference 10.
[b]R. M. Panoff and P. A. Whitlock, Can. J. Phys. **65**, 1409 (1987).
[c]Reference 25.
[d]D. M. Ceperley and E. L. Pollock, Can. J. Phys. **65**, 1416 (1987).

TABLE VII. Ground-state energies per particle in K (total E_0, kinetic K, and potential U) for a system with $N=256$.

	ρ_{eq}		ρ_{fre}	
	OSWF	OSWF+phonon	OSWF	OSWF+phonon
E_0	−6.919 (4)	−6.971 (5)	−6.324 (7)	−6.343 (5)
K	14.630 (5)	14.462 (7)	19.96 (1)	19.924 (7)
U	−21.549 (5)	−21.433 (4)	−26.284 (6)	−26.267 (6)

We therefore add a long-range tail of the form suggested in Ref. 26 to the shadow pseudopotential u_s, namely,

$$u_s(r)=u_s^{sr}(r)+u_s^{lr}(r)=u_s^{sr}(r)+\frac{1}{2}\frac{mc}{\pi^2\rho\hbar}\frac{1}{r^2+k_c^{-1}}, \tag{10}$$

where u_s^{sr} is the short-range term of Eq. (8), c is the sound velocity, and k_c is a cutoff parameter for the onset of the r^{-2} behavior. Note that in the SWF the long-range tail can be added to either u_p or u_s, or it can be split between the two; we choose u_s for consistency with the excited state wave function, discussed in the next section, which has the density-fluctuation operator acting on the shadow variables.

In periodic boundary conditions, while u_s^{sr} vanishes at half the simulation box side, $u_s^{lr}(s_{ij})$ includes the correlation between shadow i and all the images of shadow j in the periodically repeated simulation cell.[28] The long-range contribution to $\ln\Psi$,

$$-\sum_{i<j}u_s^{lr}(s_{ij})=\frac{1}{2}\sum_{\mathbf{k}\neq 0;|\mathbf{k}|<k_{max}}\hat{u}_s^{lr}(\mathbf{k})\rho_{-\mathbf{k}}\rho_{\mathbf{k}}, \tag{11}$$

is evaluated in reciprocal space: here $\mathbf{k}$ are the reciprocal lattice vectors (RLV's) of the simulation cell, $\hat{u}_s^{lr}$ is the Fourier transform of u_s^{lr}, and $\rho_{\mathbf{k}}=\Sigma_{j=1}^{N}\exp(-i\mathbf{k}\cdot\mathbf{r}_j)$ are the collective coordinates. We choose k_{max} such as to restrict the sum to the first 25 stars of RLV's.

With c given by the OSWF equation of state of Eq. (3), simulations of large ($N=256$) systems with different values of k_c have been performed at equilibrium and freezing density. Results are shown in Table VII. In both cases the energy is lowered by the phonon term and the optimal value of k_c turns out to be 0.25 Å^{-1}. The improvement in the variational upper bound for the energy is small at the freezing density but it is as large as 0.05 K at ρ_{eq}. This gives by far the best estimate of the binding energy of liquid ^{4}He, -6.971 ± 0.005 K, less than 2.5% above the experimental value.

With this wave function we can evaluate the effect of long-range correlations up to a maximum wavelength equal to the simulation box side. In particular, the static structure factor $S(k)=\langle\rho_{-\mathbf{k}}\rho_{\mathbf{k}}\rangle/N$, calculated at the RLV's for a system of $N=256$ atoms at the equilibrium and freezing density, is shown in Fig. 7. The inclusion of u_s^{lr} brings the simulation results in agreement with the predicted[26] long-wavelength behavior, $S(k)=\hbar k/2mc+O(k^2)$, as well as with experiment.

III. EXCITED STATES SHADOW WAVE FUNCTION

The SWF variational technique has been extended to study excited-states properties of superfluid ^{4}He.[12] The method is a generalization of the Feynman ansatz[3] in which a wave function for an excited state $\Psi_{\mathbf{k}}$, of momentum $\hbar\mathbf{k}$, is obtained by introducing a suitable momentum carrying factor in the ground-state wave function. The interpretation of the shadow variables as a way to represent the effect of the zero-point motion of hard-core particles suggests that this effect should be present in a similar way also in the excited states of low energy. Therefore, a natural representation of the wave function for the excited states was obtained[12] by expressing the density fluctuations in terms of the shadow variables $\sigma_{\mathbf{k}}=\Sigma_j\exp[i\mathbf{k}\cdot\mathbf{s}_j]$. The resulting structure of $\Psi_{\mathbf{k}}$ is similar to the Feynman's form, however it turns out[14] that in this wave function the density fluctuation $\sigma_{\mathbf{k}}$ induces implicitly terms of all orders in the density fluctuation of the real variables, i.e., backflow is already included and it is not limited to terms of low order in the density fluctuations $\rho_{\mathbf{k}}$.

A significant improvement over these earlier results was obtained by introducing explicit backflow terms in $\Psi_{\mathbf{k}}$.[16,17] Indeed, in the original wave function of Ref. 12 no variational parameter for the excited states is present and the form

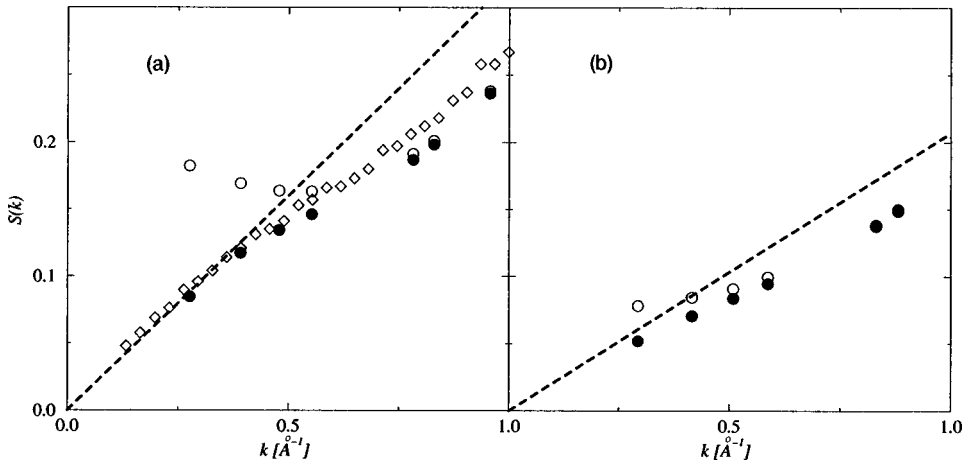

FIG. 7. OSWF $S(k)$ for liquid ^{4}He at equilibrium density (a), and at freezing density (b) with (filled circles) and without (empty circles) the phonon correction, with the sound velocity from the equation of state of Fig. 3 ($c=248$ m/s at equilibrium density, $c=383$ m/s at freezing density) and $k_c=0.25$ Å^{-1}. The solid line indicates the correct small k slope, and the diamonds are experimental results (Ref. 27).

of backflow is uniquely determined by the correlations between shadow variables,[14] i.e., by a ground-state property. It is remarkable that such a parameter–free wave function already gives good results,[12] but a more adequate $\Psi_{\mathbf{k}}$ should contain the possibility to optimize the backflow included in it. A more accurate SWF for the excited state includes an explicit backflow term and has the form[16,17]

$$\Psi_{\mathbf{k}}(R)=\Phi_p(R)\int dS\Theta(R,S)\Phi_s(S)\,\delta_{\mathbf{k}}, \tag{12}$$

where Φ_p, $\Theta(R,S)$, and $\Phi_s(S)$ are the correlating factors for the ground state while the momentum carrying factor in Eq. (12) is

$$\delta_{\mathbf{k}}=\sum_j e^{i\mathbf{k}\cdot[\mathbf{s}_j+\Sigma_{l(\neq j)}(\mathbf{s}_j-\mathbf{s}_l)\lambda(|\mathbf{s}_j-\mathbf{s}_l|)]}. \tag{13}$$

It is easy to show that this wave function is an eigenstate of linear momentum with value $\hbar\mathbf{k}$. If $\lambda(s)=0$, $\delta_{\mathbf{k}}$ is simply a density fluctuation in the shadow variables and the wave function of Ref. 12 is recovered. For $\lambda(s)$ a short-range form is assumed:

$$\lambda(s)=\begin{cases} A[(s/r_0)-2]^2e^{-[(s-r_0)/w]^2} & s\leqslant 2r_0, \\ 0 & s\geqslant 2r_0. \end{cases} \tag{14}$$

A, r_0, and w are the variational parameters for the excited state $\Psi_{\mathbf{k}}$ and their values are determined by minimization of the expectation value of the Hamiltonian; in principle their values can depend on the wave vector $\mathbf{k}$ of the excitation. With the wave function given by Eq. (12), the SWF technique is able to reproduce the excitation spectrum $E(k)$ of superfluid ^{4}He with an accuracy at the level of a good variational *ground-state* calculation.[16,17]

In the present work we repeat the computation for the excited states using the improved ground-state description afforded by the OSWF. In fact, the excitation energy is obtained as the difference between two expectation values so that there is no strict variational principle for $E(k)$. Therefore, it is important to use a wave function as good as possible. We also include the proper r^{-2} long-range correlations due to the zero-point motion of phonons, in order to address two issues that remained unsolved from the previous computations. In the first place, the excitation spectrum obtained in Refs. 16 and 17 shows the typical linear behavior expected in the phonon region but with an artificial finite-energy extrapolation at $k=0$. We can now verify if this was originated by the absence of long-range correlations in the wave function. Second, the excitation spectrum derives from the sum of the excitation kinetic energy and the excitation potential energy of the state. For a small k phonon, a harmonic oscillation of local density, there is equipartition between the two. At the smallest wave vector considered in Refs. 16 and 17 ($k=0.369$ Å^{-1}), in the region where $E(k)$ is roughly linear, no tendency to reach equipartition was observed. In the present calculation it is possible to verify whether this is an artifact due to the lack of long-range correlations, or the harmonic regime indeed sets in only at substantially smaller values of k. In this respect, additional DMC simulations are performed to exclude the possibility of a variational bias coming from the structure of the SWF.

A. Algorithm and technical aspects

The excitation energy spectrum $E(k)$ is defined as the difference between two extensive quantities: the expectation value of the total energy for the excited state of momentum $\hbar\mathbf{k}$ and that for the ground state

$$E(k)=\frac{\langle\Psi_{\mathbf{k}}|\hat{H}|\Psi_{\mathbf{k}}\rangle}{\langle\Psi_{\mathbf{k}}|\Psi_{\mathbf{k}}\rangle}-\frac{\langle\Psi|\hat{H}|\Psi\rangle}{\langle\Psi|\Psi\rangle}. \tag{15}$$

Notice that this is a very demanding task for a MC computation because $E(k)$ is typically one hundredth or less of the total energies and prior to Ref. 12 it was not clear that such a computation would be feasible.

The computation of the energy of an excited state is based on a random walk generated for the ground state. This is necessary because the square modulus of the excited-state wave function is positive definite only after integration over the shadow variables. We use the same kind of reweighting technique described for the optimization procedure of the ground state, so that the energy spectrum can be written in terms of averages over the random walk generated for the ground state in the extended space $\{R,S_L,S_R\}$ as follows:

$$E(k)=\frac{\left\langle \delta^L_{-\mathbf{k}}\delta^R_{\mathbf{k}}\dfrac{\hat{H}\Psi}{\Psi}\right\rangle_{(R,S_L,S_R)}}{\langle\delta^L_{-\mathbf{k}}\delta^R_{\mathbf{k}}\rangle_{(R,S_L,S_R)}}-\left\langle\frac{\hat{H}\Psi}{\Psi}\right\rangle_{(R,S_L,S_R)}. \tag{16}$$

$\delta^L_{-\mathbf{k}}\delta^R_{\mathbf{k}}$ is the k-dependent weight of the local energy $\hat{H}\Psi/\Psi$ defined in Eq. (4). $\delta^L_{\mathbf{k}}$ is the density fluctuation modified by backflow for shadows S_L and $\delta^R_{\mathbf{k}}$ for shadows S_R. The denominator in the first term of Eq. (16) derives from the normalization of $\Psi_{\mathbf{k}}$. All three averages in Eq. (16) are taken with respect to the same configurations generated using a standard Metropolis algorithm for the ground state with asymptotic probability given by

$$p(R,S_L,S_R)=\frac{\Phi_p(R)^2\Theta(R,S_L)\Theta(R,S_R)\Phi_s(S_L)\Phi_s(S_R)}{\displaystyle\int dRdS_LdS_R\Phi_p(R)^2\Theta(R,S_L)\Theta(R,S_R)\Phi_s(S_L)\Phi_s(S_R)}. \tag{17}$$

The reweighting technique is, on the other hand, advantageous because the fluctuation effects coming from the averages in Eq. (16) are correlated and this reduces the variance of $E(k)$.

We have studied systems composed of 256 ^{4}He atoms in a cubic box with periodic boundary conditions both at equilibrium ($\rho_{eq}=0.0218$ Å^{-3}) and freezing density ($\rho_{fr}=0.0262$ Å^{-3}). In this way the smaller wave vector compatible with the periodic boundary condition of the system is $k=2\pi/L=0.276$ Å^{-1} at ρ_{eq} (L is the side of the simulation cell) and $k=0.294$ Å^{-1} at ρ_{fr}, well inside the phonon region of the spectrum at both densities. The computation has been performed for the **k** vectors compatible with periodic boundary conditions along the principal directions (111), (110), and (100). Only around the roton minimum we have also considered **k** in other directions in order to better locate the position of this roton minimum.

Many of the allowed wave vectors **k** are equivalent. It is convenient to take the average of $\delta^L_{-\mathbf{k}}\delta^R_{\mathbf{k}}$ in Eq. (16) over the stars of equivalent **k**. Moreover, each $\delta_{\mathbf{k}}$ is a combination of trigonometric functions of the kind $\sin[2\pi/L(n_x s_i^x+n_y s_i^y+n_z s_i^z)]$ or $\cos[2\pi/L(n_x s_i^x+n_y s_i^y+n_z s_i^z)]$. It is convenient to express all these functions in terms of $\sin(2\pi s_i^{(x,y,z)}/L)$ and $\cos(2\pi s_i^{(x,y,z)}/L)$ via standard trigonometric relations in order to avoid the direct calculation of many sine and cosine functions that are more time consuming than sums or products.

In order to have an acceptable statistic for $E(k)$, the simulation has to be much longer than that necessary for the ground state. Typically, we have used runs of order of 2×10^7 Monte Carlo steps in our computation. Here one Monte Carlo step coincides with a trial move of all the $3N$ variables ($N=256$, N real, and $2N$ shadows: left and right) in the simulation cell one at a time.

With the excited-state wave function Eq. (12) one has to compute many times the excitation spectrum, one for every set of variational parameters for the excited state: $E(k)=E(k,A,r_0,w)$. This causes a large increase of the computational cost of the code with respect to the excited-state SWF that does not contain an explicit backflow contribution. Therefore, some preliminary run has to be done in order to determine the useful range of values for A,r_0,w. In any case the calculation of $E(k,A,r_0,w)$ for every combination of A,r_0,w exploits the random walk generated from the ground state that remains the most time-consuming part of the code and that is generated once for all. We have found that $E(k,A,r_0,w)$ is most sensitive to the amplitude A of the explicit backflow term; moreover, the optimal value of A depends strongly on the wave vector of the excitation. The dependence of $E(k)$ on the range parameters r_0 and w is rather weak. In order to keep the code to a reasonable computational cost, we have chosen to fix the parameters r_0 and w to the optimal value for the roton region ($r_0=2.81$ Å at both densities, $w=1.53$ Å at equilibrium density and $w=1.02$ Å at freezing density), whereas A has to be optimized at each **k**. From the point of view of the computational cost of the code, the inclusion of the long-range correlation in the ground state affects only the generation of the random walk of the ground state, but the presence of the long-range tail in the pseudopotential u_s of the shadow variables modifies the implicit backflow contained in $\Psi_{\mathbf{k}}$. This is not a problem in our computation because the backflow contribution is important only for an accurate description of the roton and maxon regions of the spectrum. For these regions it is clear that the long-range behavior of the total backflow has less importance in the description of the excited state than the short-range part that can be optimized through the explicit contribution.

Another quantity directly related to the excited state and which is possible to calculate during our simulation is the strength of the single excitation peak $Z(k)$ in the dynamical structure factor $S(k,\omega)$. The excitation spectrum is measured by inelastic neutron scattering that gives the dynamical structure factor $S(q,\omega)$. At low temperatures, $T\simeq1$ K or below, $S(k,\omega)$ consists of a sharp peak and of a broad contribution so that it is usual to decompose $S(k,\omega)$ as follows:

$$S(k,\omega)=Z(k)\,\delta(\omega-E(k)/\hbar)+S_m(k,\omega). \tag{18}$$

$Z(k)$ gives the strength of the sharp peak and S_m gives what is called the multiphonon (more properly multiexcitation) background, i.e., the contribution in which the neutron exchanges energy with two or more excitations.[29] From the sum rule

$$\int_{-\infty}^{\infty} S(q,\omega)\,d\omega=S(k)=\frac{1}{N}\langle\rho_{-\mathbf{k}}\rho_{\mathbf{k}}\rangle, \tag{19}$$

in terms of the static structure factor $S(k)$, it is clear that the ratio $f(k)=Z(k)/S(k)$ gives the efficiency of the single excitation scattering process: this important quantity is a measure of the departure of the excited state from a simple density fluctuation in the system. If the excitation were a simple density wave, as given by the Feynman wave function, this ratio would be one and this is found experimentally to be the case for $k\lesssim0.5$ Å^{-1}. $f(k)$ has a maximum but significantly below one in the roton region whereas it is minimum for maxons and at the end point where $Z(k)$ is vanishing. Standard variational theory of rotons overestimates $Z(k)$ and a typical value is 1.2.[7] From the expression of $S(k,\omega)$ it turns out that $Z(k)$ can be obtained from the formula $Z(k)=|\langle\Psi_{\mathbf{k}}|\rho_{\mathbf{k}}|\Psi\rangle|^2$. Using SWF and the reweighting technique we get

$$Z(k)=\frac{|\langle\delta^L_{-\mathbf{k}}\rho_{\mathbf{k}}\rangle_{(R,S_L,S_R)}|^2+|\langle\delta^R_{-\mathbf{k}}\rho_{\mathbf{k}}\rangle_{(R,S_L,S_R)}|^2}{2N\langle\delta^L_{-\mathbf{k}}\delta^R_{\mathbf{k}}\rangle_{(R,S_L,S_R)}}. \tag{20}$$

Sparse averaging and data blocking are the standard Monte Carlo techniques used in the calculation of $E(k)$ and $Z(k)$. From the averages and the standard deviations of the various estimators computed in the single blocks we get a measure of the statistical uncertainty of the computation. Agreement between the average of the values of $E(k)$ obtained in each single block and the final cumulative averages is an indication of the convergence of the algorithm. The configurations of the $3N$ variables have been generated at each density for the computation of $E(k)$ on a CRAY T3E with 128 processors working in parallel. The efficiency of the parallel algorithm is very high (about 100%) because we have run in parallel 128 statistically independent simulations,

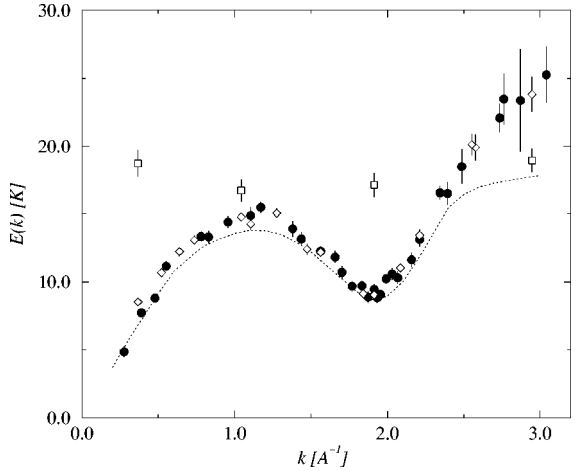

FIG. 8. (circles) Excitation spectrum computed for a system of 256 particles for a fully optimized excited state SWF that contains the long-range correlations due to the zero point motion of phonons. (diamonds) Excitation spectrum computed for a system of 108 particles for a fully optimized excited state SWF without the long-range correlations. (squares) Excitation spectrum for a double roton excitation.

spending little time in communicating the accumulated values for the various estimators only at the end of each block to calculate the averages.

B. Results

In Fig. 8 we show the excitation spectrum computed at equilibrium density with the SWF that contains the correct long-range contribution due to the zero-point motion of phonons. In this figure we also show the excitation spectrum computed in Ref. 17 for a system of 108 particles without this contribution but with the correlation functions optimized with the basis set method. We can see that the new $E(k)$ has the correct behavior for small k. This indicates that in Ref. 17 the wrong behavior of $E(k)$ in the phonon region was due to the absence of the long-range part in the pseudopotentials. This is what we find also at freezing density. At this density the computed energy spectrum can be seen in Fig. 9. Upon changing the density of the system, all the experimental features of $E(k)$ are reproduced by our theory: the roton energy

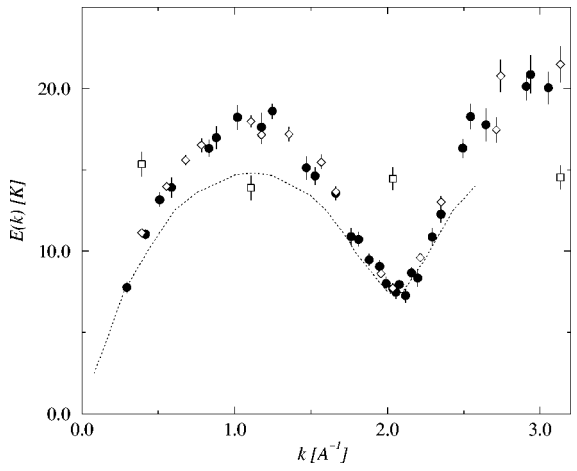

FIG. 9. The same as Fig. 8 at freezing density.

TABLE VIII. Roton energies in K.

	Short range (Ref. 17)	Long range	Expt. (Ref. 30)
ρ_{eq}	9.05 (29)	9.04 (16)	8.61 (01)
ρ_{fre}	7.73 (25)	7.59 (18)	7.30 (02)

decreases and the maxon $E(k)$ increases at the larger density and the roton wave vector is displaced to a larger value. Therefore, not only the maxon and roton energies are very satisfactory but also the corresponding k vectors. Note that the only input in this microscopic calculation is the interatomic interaction between ^{4}He atoms. One can also see that the inclusion of the long-range contribution to pseudopotentials affects only the phonon region of the excited spectrum. In Table VIII we report the roton energies found in the present computation to be compared with our previous results[17] obtained with short-range pseudopotentials and with the experimental values.[30] In the present computation we have $E(k)$ for many more values of $\mathbf{k}$ in the roton region but the statistical uncertainty in $E(k)$ is still too large to extract a meaningful effective mass for the roton.

As already found in Ref. 17, the energy of the state with SWF (12) is in significant disagreement with experiment in two cases: at large q above 2.5 Å^{-1} and in the maxon region at the freezing density. Outside these regions the deviation from experiment at both densities is of the order of 5% at all wave vectors. In the k regions where there is a significant disagreement between our results and the experimental data, the experimental $E(k)$ is about twice the roton energy so that we might expect that these excitations are a mixture of single and double excitations. The relevance of this argument was proved in Ref. 17 where the computation has been extended to a double roton excited state. This is obtained by replacing in Eq. (12) $\delta_{\mathbf{k}}$ by $\delta_{\mathbf{q}}\delta_{\mathbf{k}-\mathbf{q}}$, q and $|\mathbf{k}-\mathbf{q}|$ being equal to the roton wave vector. The SWF for this double roton excited state is then given by

$$\Psi_{\mathbf{k}}(R)=\Phi_p(R)\int dS\Theta(R,S)\Phi_s(S)\,\delta_{\mathbf{q}}\delta_{\mathbf{k}-\mathbf{q}}. \qquad (21)$$

Using the reweighting technique, the spectrum $E_{db}(k)$ of this excitation can be computed through the formula

$$E_{db}(k)=\frac{\left\langle \delta^L_{-\mathbf{q}}\delta^L_{\mathbf{q}-\mathbf{k}}\delta^R_{\mathbf{q}}\delta^R_{\mathbf{k}-\mathbf{q}}\dfrac{\hat{H}\Psi}{\Psi}\right\rangle_{(R,S_L,S_R)}}{\langle \delta^L_{-\mathbf{q}}\delta^L_{\mathbf{q}-\mathbf{k}}\delta^R_{\mathbf{q}}\delta^R_{\mathbf{k}-\mathbf{q}}\rangle_{(R,S_L,S_R)}} -\left\langle\frac{\hat{H}\Psi}{\Psi}\right\rangle_{(R,S_L,S_R)}. \qquad (22)$$

The results obtained in Ref. 17 for few values of k are also reported in Figs. 8 and 9. Where the computed spectrum $E(k)$ is in significant disagreement with the experimental data, the energy of a double excitation is below the one of the single excitation and close to experiment. This proves that under these conditions $\Psi_{\mathbf{k}}$, given in Eq. (12), is not a good representation of the excited state and a mixture of states should be considered. The results for the double roton excitation has been obtained with a SWF that does not in-

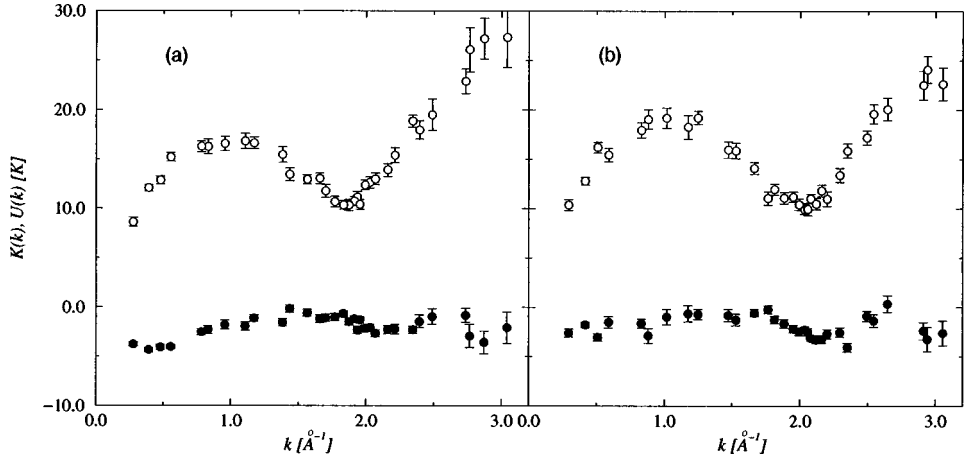

FIG. 10. (a) Kinetic excitation energy (filled circles) and potential excitation energy (open circles) for a fully optimized SWF that includes the long-range correlations, at equilibrium density. (b) The same as (a) at freezing density.

clude the long-range correlations due to the zero-point motion of phonons. This however is not a problem because we have seen that these correlations do not affect the excited states built with density fluctuation in which the wave vector is in the roton region.

We have computed separately the kinetic $K(k)$ and the potential $U(k)$ contribution to the excitation spectrum and the results are shown in Fig. 10 for equilibrium and freezing density. We see that the potential energy contribution to $E(k)$ has the tendency to be negative and it has a negative minimum in the roton region or slightly beyond it. In our theory the roton energy of about 9 K at equilibrium density corresponds to about -1.5 K of potential energy and to 10.5 K of kinetic energy. At freezing the potential energy of a roton is -3 K and the kinetic energy is 10.6 K so that most of the depression of the roton energy at the larger density is due to the lowering of the potential energy. These findings are in agreement with an earlier computation based on SWF,[31] where the negative contribution of the potential energy to the energy of a roton was shown to be due to an enhanced short-range order in the excited state. This, in fact, has been related to the experimental observation that the height of the main peak of $S(k)$ is an increasing function of temperature in the superfluid phase of ^{4}He.[32]

We now consider the region of small wave vectors. From Fig. 10 we can see that $U(k)$ is negative also in the phonon region where $E(k)$ is roughly linear. Therefore there is still no tendency to reach equipartition even if the excited-state wave function includes the long-range contribution due to the zero-point motion of phonons. This point will be further discussed in the next subsection where comparison between these results and those obtained from a DMC calculation within the fixed node approximation will be presented.

In Fig. 11 we show our results for the static structure factor $S(k)$ and for the strength $Z(k)$ of the single excitation peak in $S(k,\omega)$ both at freezing and equilibrium densities. The result for the relative strength of this peak, i.e., $f(k) = Z(k)/S(k)$ is compared with experiment in Fig. 12. There is a good agreement especially with recent results,[33] and this is important because this quantity is rather sensitive to the structure of the wave function. The present theory appears to be the first one able to give a quantitative description of $Z(k)$ in the roton region. $f(k)$ in the roton region is almost density independent, but in the maxon region there is a significant decrease of $f(k)$ at the higher density. This is also what is found experimentally.[33] $f(k)$, especially in the maxon region, is very sensitive to the backflow contained in SWF (12), more than what is found for $E(k)$; the irregularities in

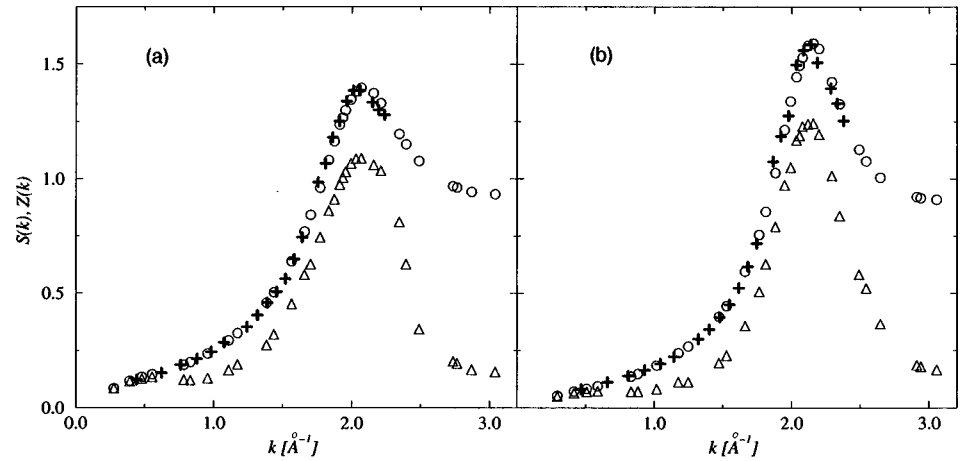

FIG. 11. (a) Static structure factor (open circles) $S(k)$, strength of the single excitation peak (triangles) $Z(k)$ at equilibrium density. (plus) DMC results for $S(k)$. (b) The same as (a) at freezing density.

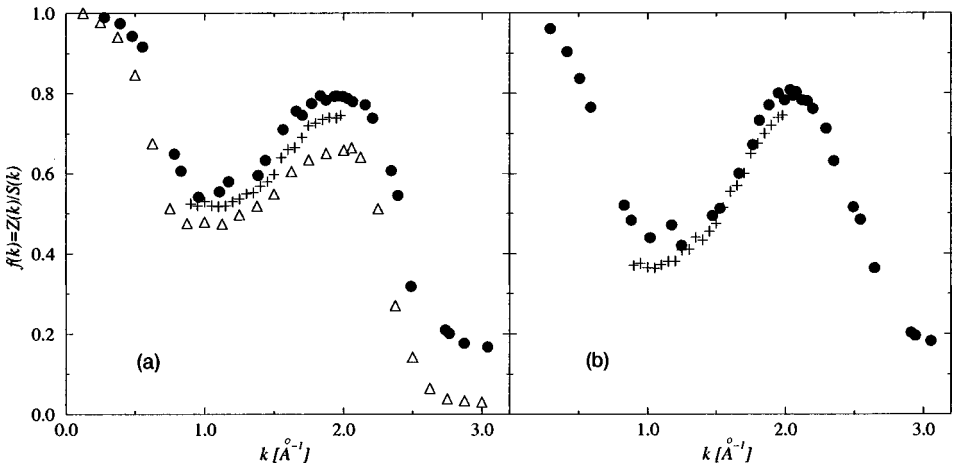

FIG. 12. (a) $f(k)=Z(k)/S(k)$ computed at equilibrium density (filled circles) compared with recent experimental data (plus) (Ref. 33) and experimental data (Ref. 6). (b) The same as (a) at freezing density.

Fig. 12 are therefore due to the discrete set of values of the amplitude of the explicit backflow contribution used in the MC simulation. As can be seen in Fig. 11 the long-range contributions due the zero-point motion of phonons strongly affects the results of $Z(k)$ in the phonon region where the excitations are simple density fluctuations and therefore $Z(k)\rightarrow S(k)$ for $k\rightarrow 0$. In this region we now have a good description also for $Z(k)$. It should be noticed that $Z(k)$ and $f(k)$, given by the present theory, are not reliable in the k regions where, as discussed above, the energy of a double roton excitation is below that of the single excitation.

C. Long-wavelength excitations

The variational study of the phonon-maxon-roton spectrum with the SWF yields the unexpected result, shown in Fig. 10, that equipartition between kinetic and potential energy of the phonon is far from being fulfilled even for wave vectors down to ~ 0.2 Å^{-1}, where the excitation energy exhibits a nearly linear dispersion (see Fig. 10). We now present results obtained with the fixed node diffusion Monte Carlo (FNDMC) method that support, in this respect, the reliability of the variational calculation.

Although the implementation of DMC with SWF is possible,[34] here we follow the standard approach and use the OJOT wave function,[2] supplemented by the correct long-range tail[26] in the pair correlation, as the trial function Ψ of the ground state. For the excited state we take a linear combination

$$\Psi_{\mathbf{k}}(R)=\frac{1}{2}(\rho_{-\mathbf{k}}+\rho_{\mathbf{k}})\Psi(R)=\sum_i \cos(\mathbf{k}\cdot\mathbf{r}_i)\Psi(R) \qquad (23)$$

of two degenerate excitations, so that the trial function is real, which is convenient for the DMC simulation.

The DMC algorithm gives the *exact* energy of the Boson ground state. For the excited state the wave function is not positive, and the *sign problem* makes the exact algorithm unstable. We avoid this problem by forcing the random walks not to cross the nodes of the trial function: this is the FN approximation, which consists of assuming that the true excited state and the trial function $\Psi_{\mathbf{k}}$ have the same nodes.[35] Such an assumption is certainly not correct for the simple form of Eq. (23) that neglects backflow, and a recent DMC calculation[36] of the excitation spectrum shows that even improving the nodal structure with the inclusion of backflow correlations in the form of Eq. (13), the FN approximation gives poor results for the maxon and roton energies.

Nevertheless, the FN bias vanishes as the nodal structure of the trial function becomes exact, which is precisely what we expect in the long-wavelength region of interest in this context: we will resort to the comparison with the experimental excitation energy to establish the range of wave vectors where the FNDMC calculation is reliable, and we will examine the behavior of the potential and kinetic excitation energies in this range.

We also note that the nodal structure of excited states lacks, in general, the tiling property,[35] and a further bias may be introduced depending on which nodal pockets have been populated at the beginning of the simulation. Indeed, we found occasionally slightly different results from different sets of simulations, the effect being however small for the purpose of the present discussion.

DMC simulations are performed for 64 atoms in a cubic box and for 128 atoms in a box with $L_x=L_y=L_z/2$, at equilibrium density. Since a direct application of the reweighting method to the DMC configurations is not possible, we take energy differences between independent runs for the excited and the ground state. Results are complemented by variational simulations with the OJOT wave function; the latter are extended also to a system of 256 atoms in a box with $L_x=L_y=L_z/4$, whose smallest RLV is 0.11 Å^{-1}, using the reweighting method. We use such elongated simulation boxes in order to reach smaller wave vectors than would be allowed by a cubic box with the same number of particles. Comparison between results obtained with boxes of different shape shows that the excitation energies are not affected by geometrical factors.

The results for $E(k)$ are shown in Fig. 13. The VMC excitation spectrum closely follows the Feynman approximation,[3] $E(k)=\hbar^2/[2mS(k)]$, where for the static structure factor the result of the same VMC calculation has been used. This is an expected result, in view of the fact that the excited state is of the Feynman form (23), and indicates that the OJOT wave function with the correct long-range tail

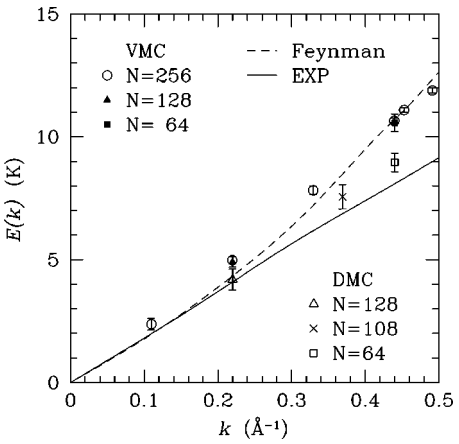

FIG. 13. Excitation spectrum of liquid ^{4}He at equilibrium density calculated by VMC and FNDMC with the trial function of Eq. (23) for the excited state. The FNDMC result at $k=0.369$ is taken from Ref. 37. Experimental data and the Feynman approximation are shown as well.

is a good representation of the ground state. Note that the Feynman approximation becomes exact in the long-wavelength limit. The DMC calculation gives improved results, and comes in agreement with experiment at $k=0.22$ Å^{-1}. For this wave vector the potential energy of the excitation, shown in Fig. 14, is still negative. The variational calculation, which also appears to be accurate at small k from the comparison with both DMC and experimental data, shows that the potential energy becomes positive only for wave vectors less than 0.1 Å^{-1}.

To summarize, we judge the accuracy of the FNDMC calculation on the basis of the comparison with the experimental excitation energy, which is favorable for long wavelength, say, $k \lesssim 0.2$ Å^{-1}. In this range, we can assume that a corresponding accuracy is guaranteed by the algorithm also for the kinetic and potential energies separately, and they are still far from equipartition. This in turn supports the findings obtained by the variational method with either the OSWF or the OJOT wave function: the fact that the harmonic regime sets in at exceedingly small wave vectors appears to be a robust result. From the present calculations we infer that equipartition is only reached at a wave vector below 0.05 Å^{-1} or at a wavelength larger than 120 Å, about 50 times the atomic diameter. It is a totally unexpected result that the macroscopic limit is reached only at such large distances.

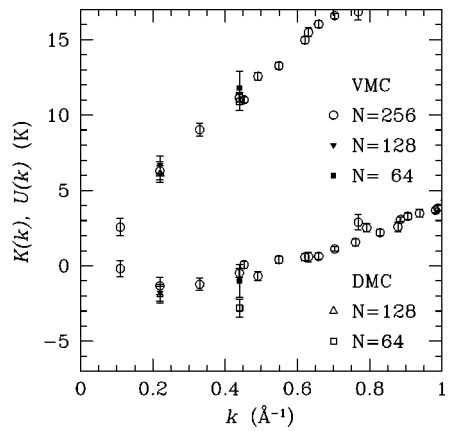

FIG. 14. Kinetic and potential excitation energy of liquid ^{4}He at equilibrium density calculated by VMC and FN-DMC with the trial function of Eq. (23) for the excited state. The FN-DMC results are *mixed estimators* (Ref. 20).

IV. CONCLUSION

We have presented an extensive study based on the shadow wave function technique of the ground state of liquid and solid ^{4}He and of the main excited states in the liquid phase. Our results confirm that the SWF approach is a very powerful technique to handle strongly interacting bosons: presently it provides the most accurate variational description of the ground-state energy of ^{4}He both in the liquid and in the solid phase as well as of the phonon-maxon-roton excitation spectrum. The typical accuracy is 3% for the ground state and 5% for the excited states. The quality of the results is not limited to the energetics but it includes quantities like the pair distribution function, the Bose-Einstein condensate fraction or, for the excited states, the strength of the single excitation peak in $S(k,\omega)$.

One aspect, rather remarkable of SWF, is its uniform accuracy in the description of the properties of ^{4}He as a function of density. It is well known to the many-body practitioners how all standard techniques find increasing difficulties in treating a strongly interacting system as the density is increased. With respect to the ground state, the deviation of Jastrow as well of Jastrow plus triplet energy from the correct value is a strongly increasing function of density. With respect to roton excitation, to recover the simple fact that the roton energy at freezing is smaller than equilibrium took quite substantial effort from many-body theory.[37] The situation is quite different with SWF. At equilibrium density SWF with short-range correlations overestimates the ground-state energy by 0.19 K, the difference is 0.18 K at freezing density and 0.19 K in the solid at melting. The roton energy is overestimated by 0.43 K at ρ_{eq} and by 0.29 K at freezing density.

It seems clear that SWF must contain some of the important features that govern the behavior of the system as the entanglement of the particles become so strong that the localized regime of the solid is approached. We believe that this is not unrelated to the fact that the same wave function is able to describe also this solid phase when the density is large enough. The technique of subsidiary variables embodied in the SWF can be seen as a mathematical way to allow for correlations in the wave function beyond the pair and triplet level. The uniform accuracy in the description of ^{4}He as a function of density suggests that in SWF there is more than a simple mathematical trick and that the shadow variables have some physical relevance. We find particularly attractive the analogy with a path-integral representation in which a shadow variable is related to the center of mass of a fragment of a path integral of a particle. This view led to the suggestion[9] that the shadow pseudopotential should contain an attractive part and this is verified by the present computation. This interpretation gives also an explanation of our result that the pseudopotentials are rather density independent within the liquid or within the solid phase but there is a significant jump as one moves from one phase to the other. In fact, the paths in which a quantum particle is mapped are

qualitatively rather different in the solid phase, in which a path will be strongly localized around an equilibrium position, with respect to the paths in a fluid where no such localization is present. In the first case we can expect a rather Gaussian-like particle-shadow correlation as it is found in the present computation, whereas a more complex behavior can be expected in the liquid phase.

In the SWF the localization of particles arises via interparticle correlations as a phenomenon of spontaneously broken symmetry. In the perspective of SWF the Gaussian localization factors that are introduced in the standard theory of quantum solids are nothing but a mean-field representation of the many-particle correlations implicitly present in the SWF. The fact that SWF is as accurate as the standard wave function in a solid at high density, and is superior at the lowest densities close to melting, has an important implication. In fact, the study of disorder phenomena in a quantum solid was essentially out of reach of variational theory in the standard formulation. These phenomena can be treated in a very natural way by SWF because Bose symmetry is guaranteed at the outset and the relaxation of equilibrium position is automatically included. Some applications of SWF to study the liquid-solid interface and a vacancy in the crystal have been already performed. The accuracy of SWF in treating the bulk solid, as found in the present work, is also a good basis for an accurate treatment of disorder phenomena in the solid.

In the present treatment of the ground state we have also included the long-range correlations due to the zero-point motion of phonons. The effect on the ground-state energy is small as expected, but it is gratifying that it is in the direction of lowering the energy.

The presence of these long-range correlations is important when excited states are considered. Only in this case one finds the expected linear behavior of the excitation energy in the phonon region. Also, this is not unexpected but this is the first time within variational MC in which a consistent description of the full phonon-maxon-roton excitation is achieved. As mentioned above, the typical deviation of the excitation spectrum from experiment is 5%, both at equilibrium and at freezing density. We would like to point out that within the Feenberg form the presently best wave function for the ground state, the OJOT one, overestimates the ground-state energy at freezing density by 9%, about three times larger than the value of OSWF for the ground state and almost twice our result for the roton energy. This gives a measure of the improvement of the variational theory obtained with SWF.

The experimental excitation spectrum $E(k)$ has a small deviation from linearity in k up to a rather large value of k, of order of 0.6 Å^{-1}. This excitation appears to be the extension to microscopic k of sound waves, i.e., of harmonic density fluctuations. Therefore, we were rather surprised by some earlier results in which no tendency was found for the excited state to reach equipartition between potential and kinetic energy. This result is confirmed in the present SWF computation in which the long-range phonon correlations are included in the ground state and the size of the system is increased so that the lowest k is 0.25 Å^{-1} (at ρ_{eq}). In order to assess the accuracy of this result, we have complemented the SWF computation of the phonon excited states with a DMC computation with fixed nodes (Feynman nodes) as well as a variational computation of the Feynman form with the OJOT ground state. These different computations mutually agree that there is a wide range of k values in which $E(k)$ is essentially linear but there is no equipartition between kinetic and potential energy. This is still true at the lowest k value (0.1 Å^{-1}) we could reach in our simulation and we can infer that equipartition is reached only at 0.05 Å^{-1}. This corresponds to a wavelength in excess of 100 Å, so that there is a substantial range of long-wavelength phonons in which these excitations are not harmonic density fluctuations as indicated by the macroscopic theory. This unexpected result calls for further investigation.

We should mention some negative aspects of SWF. The introduction of the subsidiary variables slows down significantly the convergence of a MC run and rather long autocorrelation effects set in in the presence of the attractive intershadow correlations. In addition, the zero variance property is no more satisfied and, in fact, we have been able to achieve only a partial optimization of the intershadow pseudopotential.

With respect to future developments, we expect that SWF will be very useful in situations in which a quasicrystalline order sets in, like in adsorbed phases on strong binding substrates or around impurities like positive ions. Up to now the SWF technique has been only applied to ^{4}He, which is characterized by an almost impenetrable core. It is known also that soft-core potentials, like the Coulombic one, develop rather strong short-range correlations under suitable conditions, in particular when the freezing transition is approached. We expect the SWF will be rather useful also in these cases. Finally, we should mention the application of SWF to fermions, like ^{3}He. How to formulate a proper SWF for fermions is already known[11] and some preliminary computation gives very promising results. We expect that this will be a major area of development of SWF.

ACKNOWLEDGMENTS

This work was supported by the INFM under Progetto di Supercalcolo. It was conducted in part using the CINECA supercomputer resources (T3E).

[1] E. Krotscheck, Phys. Rev. B **33**, 3158 (1986).
[2] S. Moroni, S. Fantoni, and G. Senatore, Phys. Rev. B **52**, 13 547 (1995).
[3] R. P. Feynman, Phys. Rev. **94**, 262 (1954).
[4] M. Saarela and J. Suominen, in *Condensed Matter Theories*, edited by J. Keller (Plenum, New York, 1989), Vol. 4, p. 377.
[5] E. Krotscheck, Phys. Rev. B **31**, 4258 (1985).
[6] R. A. Cowley and A. D. B. Woods, Can. J. Phys. **49**, 177 (1971).
[7] M. Manousakis and V. R. Pandharipande, Phys. Rev. B **30**, 5062 (1984); *ibid.* **33**, 150 (1986).
[8] S. Vitiello, K. Runge, G. V. Chester, and M. H. Kalos, Phys. Rev. B **42**, 228 (1990).

[9] L. Reatto and G. L. Masserini, Phys. Rev. B **38**, 4516 (1988).
[10] T. McFarland, S. Vitiello, L. Reatto, G. V. Chester, and M. H. Kalos, Phys. Rev. B **50**, 13 577 (1994).
[11] For a review, see L. Reatto, in *Progress in Computational Physics of Matter*, edited by L. Reatto and F. Manghi (World Scientific, Singapore, 1995), p. 43; M. H. Kalos and L. Reatto, *ibid.* p. 99.
[12] W. Wu, S. A. Vitiello, L. Reatto, and M. H. Kalos, Phys. Rev. Lett. **67**, 1446 (1991).
[13] S. A. Vitiello, L. Reatto, M. H. Kalos, and G. V. Chester, Phys. Rev. B **54**, 1205 (1996).
[14] L. Reatto, S. A. Vitiello, and G. L. Masserini, J. Low Temp. Phys. **93**, 879 (1993).
[15] M. Sadd, G. V. Chester, and L. Reatto, Phys. Rev. Lett. **79**, 2490 (1997).
[16] D. E. Galli, L. Reatto, and S. A. Vitiello, J. Low Temp. Phys. **101**, 755 (1995).
[17] D. E. Galli, E. Cecchetti, and L. Reatto, Phys. Rev. Lett. **77**, 5401 (1996).
[18] R. A. Aziz, V. P. S. Nain, J. S. Carely, W. L. Taylor, and J. T. Conville, J. Chem. Phys. **70**, 4330 (1979).
[19] A pseudopotential $u_x(r)$ not vanishing at $r=L/2$, where L is the simulation box side, is redefined as $\overline{u_x}(r)=u_x(r)+u_x(L-r)-2u_x(L/2)$; x denotes either p or s.
[20] D. M. Ceperley and M. H. Kalos, in *Monte Carlo Methods in Statistical Physics*, edited by K. Binder (Springer, New York, 1979).
[21] C. M. Umrigar, K. G. Wilson, and J. W. Wilkins, Phys. Rev. Lett. **60**, 1719 (1988).
[22] A. J. Williamson, S. D. Kenny, G. Rajagopal, A. J. James, R. J. Needs, L. M. Fraser, W. M. C. Foulkes, and P. Maccalum, Phys. Rev. B **53**, 9640 (1996).
[23] D. M. Ceperley, G. V. Chester, and M. H. Kalos, Phys. Rev. B **17**, 1070 (1978).
[24] F. Pederiva, G. V. Chester, S. Fantoni, and L. Reatto, Phys. Rev. B **56**, 5909 (1997).
[25] S. Moroni, S. Fantoni, and G. Senatore, Phys. Rev. B **55**, 1040 (1997).
[26] L. Reatto and G. V. Chester, Phys. Rev. **155**, 88 (1967).
[27] R. B. Hallock, Phys. Rev. A **5**, 320 (1975).
[28] D. M. Ceperley, Phys. Rev. B **18**, 3126 (1978).
[29] P. Nozières and D. Pines, *Theory of Quantum Liquids* (Addison-Wesley, Redwood, 1990), Vol. 2.
[30] W. G. Stirling, in *Excitations in Two-Dimensional and Three-Dimensional Quantum Fluids*, edited by A. G. F. Wyatt and H. J. Lauter (Plenum, New York, 1991).
[31] G. L. Masserini, L. Reatto, and S. A. Vitiello, Phys. Rev. Lett. **69**, 2098 (1992).
[32] H. N. Robkoff, D. A. Ewen, and R. B. Hallock, Phys. Rev. Lett. **43**, 2006 (1979); F. H. Wirth and H. N. Robkoff, Phys. Rev. B **35**, 89 (1987); V. F. Sears and E. C. Svensson, Phys. Rev. Lett. **43**, 2009 (1979); E. C. Svensson, V. F. Sear, A. D. B. Woods, and P. Martel, Phys. Rev. B **21**, 3638 (1980).
[33] R. M. Cravecoeur, H. E. Smorenburg, I. M. de Schepper, W. Montfrooij, and E. C. Svensson (unpublished).
[34] S. A. Vitiello and P. A. Whitlock, Phys. Rev. B **44**, 7373 (1991).
[35] D. M. Ceperley, in *Recent Progress in Many-Body Theories*, edited by J. Zabolitzky (Springer, New York, 1981); J. Stat. Phys. **63**, 1237 (1991).
[36] J. Boronat and J. Casulleras, Europhys. Lett. **38**, 291 (1997).
[37] C. E. Campbell, in *Two-Dimensional and Three-Dimensional Quantum Fields* (Ref. 30).